Indian Journal of Chemistry
Vol. 63, December 2024, pp. 1207-1221
DOI: 10.56042/ijc.v63i12.12723

Synthesis of diversely substituted 5-methylpyrazolo[1,5-*a*]pyrimidines assisted by ultrasound in aqueous media: Molecular docking for potential antiviral, anticancer activities

Shunan Kaping[a], Rene Barbie Browne[b] & Jai N Vishwakarma*[a]

[a] Organic Research Laboratory, Department of Chemistry, Assam Don Bosco University, Tapesia Gardens, Sonapur 782 402, Assam, India

[b] Department of Bio-Sciences, Assam Don Bosco University, Tapesia Gardens, Sonapur 782 402, Assam, India
E-mail: jnvishwakarma19@gmail.com, shunankaping@yahoo.in, brownrenebarbie747@gmail.com

Received 24 July 2024; accepted (revised) 27 November 2024

5-Methylpyrazolo[1,5-*a*]pyrimidine derivatives have been synthesized with starting materials that are either commercially or easily available. This is achieved by the ultrasonication of 3-amino-1*H*-pyrazoles (**3**-**7**) and enaminones (**2**) assisted by $KHSO_4$ in aqueous medium. The structures are established by spectral and analytical techniques. An X-ray crystallographic study of compound *N*-(1,5-dimethyl-3-oxo-2-phenyl-2,3-dihydro-1*H*-pyrazol-4-yl)-7-(4-methoxyphenyl)-5-methylpyrazolo[1,5-a]pyrimidine-3-carboxamide (**8b**) confirms the structural orientation and eliminates any ambiguity pertaining to its regioselectivity. Its space group is P21/n with the following unit cell parameters: a = 17.5775 (8), b = 7.1707 (4), c = 18.113 (1) Å, β = 91.449 (2) and Z = 4. Crystal structure is solved to a final R value of 0.062 and to a GOOF value of 1.09. Molecular docking of the compounds has been executed to identify the potential antiviral and anticancer agents. Moreover, molecular dynamics simulation study of the ligand **9c** in a complex with 3pp0, reveals the stability of the potential ligand candidate **9c**.

Keywords: Pyrazolo[1,5-*a*]pyrimidines, X-ray crystallography, Molecular docking, Ultrasonication

Pyrazolo[1,5-*a*]pyrimidines (PPs) have since long proven to be an alluring N-heterocyclic fused motif, showcasing remarkable potential in diverse scientific disciplines. The core pyrazolopyrimidine formed by the amalgamation of pyrazole and pyrimidine system imparts a structural superiority, offering an exceptional platform for modifications, substitutions and functionalization techniques[1]. PP derivatives, owing to their resemblance to purine systems, hold significant relevance across various biological realms for its diverse pharmacological activities particularly as potent agents in anti-tumor, antibacterial, and hepatitis C virus inhibition[2]. PPs also possess therapeutic properties like anti-leishmanial[3] anticancer[1,4], antioxidant[5,6], serotonin antagonist[7], antimicrobial[8], anti-inflammatory[9,10], anti-proliferative[11] and as fungicides[12]. This distinctive molecular architecture also forms the backbone of drugs such as allopurinol, zaleplon, indiplon, dinaciclib, dorsomorphin, ocinaplon, anagliptin, lorediplon and pyrazophos, sildenafil, tisopurine[4,13-21]. PPs demonstrated a remarkable aptness to inhibit a diverse array of protein kinase enzymes[22] like Src kinase, CDK, CHK1, B-Raf, aurora-A, KDR[23] and act as EGFR/HER2 kinase inhibitors[22], selective PI3Kδ inhibitors[24], α-glucosidase inhibitors[25] and Bcl2 inhibitors[26]. Recently, they have gained momentousness in the realm of material sciences owing to their exceptional photophysical properties[27] and in solid-state, for their notable conformational and supramolecular phenomena[27-29]. Lately, a novel category of PPs has shown superior effectiveness to ciprofloxacin with drug-like properties according to Swiss ADME and drug-likeness model scores[30].

Substituents around the PP core greatly influence and modify the biological properties of compounds exhibiting antitumoral and enzymatic inhibitory activity[25]. The presence of electron donating groups at C-2 result in improved biological activity in contrast to electron withdrawing groups[27]. Also, the selectivity and pharmacokinetics of a range of 5- (with amines linked through NH or O) and 7-substituted (arylsulfones at 7-position NH) PP possessing CDK2 inhibitory activity[31,32] have been investigated. The structure activity relationship (SAR) study *via* high throughput screening for 3-, 5-, and 7-substituted PPs

revealed that amide groups with *N*-phenyl or electron-withdrawing substituents enhance Gcase activity[33]. SAR studies revealed that the carbonyl group at C-3 interacts with the enzyme, and the amide NH restricts binding conformation[34]. It was found that the high anticancer potential achieved for PPs are partly attributed to the π–π interactions between pyrazolo[1,5-*a*]pyrimidine ring and enzymatic pocket. Also, aliphatic groups increase affinity with some enzymes, like Kinase Insert Domain Receptor[25]. In addition, introduction of a methyl group at C-6 yielded promising potency enhancement while maintaining a good ligand efficiency and its presence at C-5 led to appreciable potency[34].

Exploring the remarkable versatility and broad therapeutic potential inherent in pyrazolo[1,5-*a*]pyrimidines, we have recently unveiled the synthesis and evaluated these intriguing compound's diverse biological properties[35-38] (Fig. 1). In continuation of these studies by our group and others described in the literature and also driven by their compelling impact on the development of drugs with potent anticancer and notable antibacterial activities[39], we herein report a novel series of pyrazolo[1,5-*a*]pyrimidines with a methyl group embedded at C-5 of the pyrazolopyrimidine core. Molecular docking approach was employed for determining the interaction of the compounds with target proteins to determine the most suitable configuration with the lowest binding energy[40].

Ever since the outbreak of the COVID-19 pandemic, COVID-19 main protease (PDB-ID 6LU7) has been considered one of the viable targets for antiviral drug discovery[41-44]. Its structure has been extensively studied and characterized, providing valuable insights for rational drug design[45] and identifying potential binding sites for small molecule inhibitors. Given the urgency of the COVID-19 pandemic, targeting the main protease allows for a focused approach to drug development efforts, facilitating the synthesis and testing of ligands, making it a primary target for antiviral studies. This led to the selection of COVID-19 main protease as the target protein for antiviral studies.

Likewise, for the anticancer activity, the target HER 2 Protein of Oral Cancer (PDB-ID 3PP0) was chosen for molecular docking studies due to its pivotal role in cancer biology. From the literature review, it was reported that the human epidermal growth factor receptor (HER) family is central to the pathogenesis of several human cancers. They regulate cell growth, survival, and differentiation *via* multiple signal transduction pathways and participate in cellular proliferation and differentiation. The family is made up of four main members: HER 1, HER 2, HER 3, and HER 4 respectively[46]. HER 2 is expressed in many tissues and its major role in these tissues is to facilitate excessive or uncontrolled cell growth and tumorigenesis. Overexpression of HER 2 is linked to cancers like ovary, endometrium, bladder, lung,

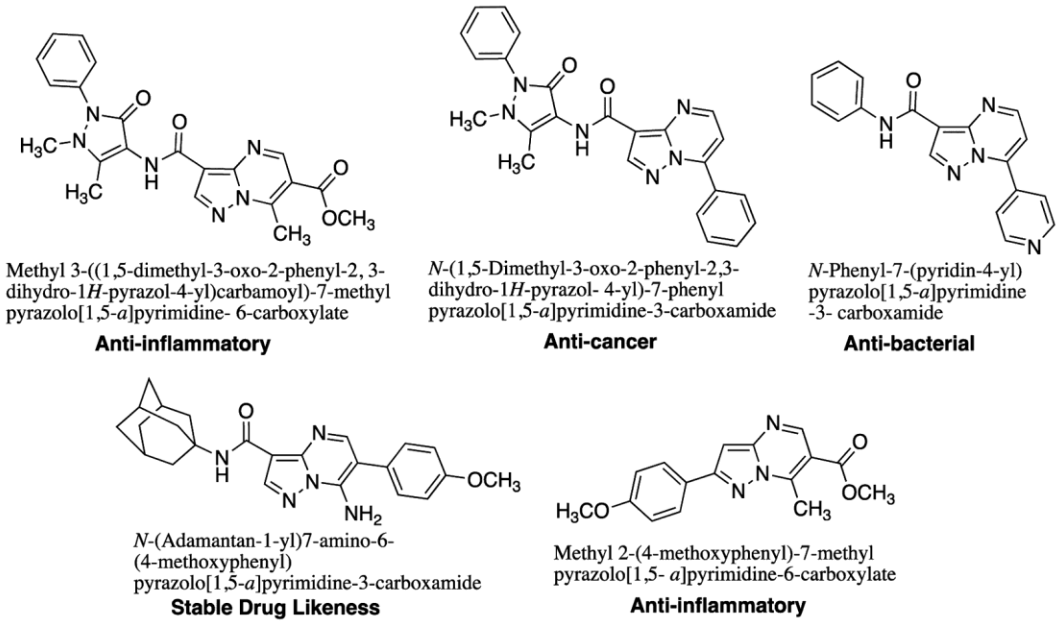

Fig. 1 — Reported pyrazolo[1,5-*a*]pyrimidines with biological activities

colon, head and neck[47-50]. Continued research on HER 2 biology and targeted therapies has led to the development of novel treatment strategies and therapeutic agents, driving innovation in drug discovery for HER 2-positive cancers.

Thus, we have conducted *in silico* molecular docking and molecular dynamics simulation to identify the most promising drug candidates exhibiting potent antiviral and anticancer, properties.

Experimental Section

Chemistry

Melting points were recorded by open capillary method using Büchii B-540 and are uncorrected. The IR spectra were recorded on a Perkin-Elmer 983 spectrometer (Perkin-Elmer). ^{1}H and ^{13}C NMR spectra were recorded on a JEOL JNM-ECS 400 taking Me_4Si as the internal standard in $CDCl_3$. In the NMR spectral data, the abbreviations d, s, m, and t, stand for doublet, singlet, multiplet, and triplet, respectively. The electron spray mass spectra were recorded on a THERMO Finnigan LCQ Advantage max ion trap mass spectrometer. HRMS data were recorded by mass analyser of model – Xevo G2-XS QTof, Make-Walters, Software-MassLynx V 4.1. Ultrasonication was carried out in an EQUITRON Digital Ultrasonic Cleaner–2.5 litre, model 8425.025.424 at 170 watt and 50 Hz. Acylated active proton compounds (**56**) were synthesized by our previously reported procedure[51]. The structures were solved by direct methods (SHELXL)[52] and refined by full-matrix least-squares based on F2 using anisotropic displacement parameters. All the non-H atoms were refined in the anisotropic approximation: H-atoms were located at calculated positions. The structures were drawn using Olex2 software[53]. The crystallographic data for the structure were deposited to the Cambridge Crystallographic Data Center with CCDC no. 2312662. 3-Aminopyrazoles **3**, **4**, **6**, **7** required for the synthesis of the target pyrazolo[1,5-*a*]pyrimidines had been synthesized as per our previous reported work[35-38]. 3-Aminopyrazole **5** was obtained from commercial sources.

General Procedure

Synthesis of 3-substituted-5-methyl-7-arylpyrazolo[1,5-a] pyrimidines, 8-10

A mixture of acetophenone **1** (1 mmol) and *N*, *N*-dimethylacetamide dimethyl acetal (DMA-DMA, 2 mmol) in xylene (2.5 mL) was refluxed for 20 h and at the end of the reaction (TLC), the solvent was removed under reduced pressure to give practically pure product **2**[51]. To this, was added 3-amino-1*H*-pyrazole **3/4/5** (1 mmol) and dissolved in 2.5 mL EtOH. Subsequently, a solution of $KHSO_4$ (2 mmol) in 2.5 mL of water was added to it in one lot and the resulting mixture was irradiated in ultrasonic bath at 60°C. The reaction went to completion within 2–10 minutes (TLC) (Scheme 1). At the end of the reaction, the mixture was allowed to cool and the

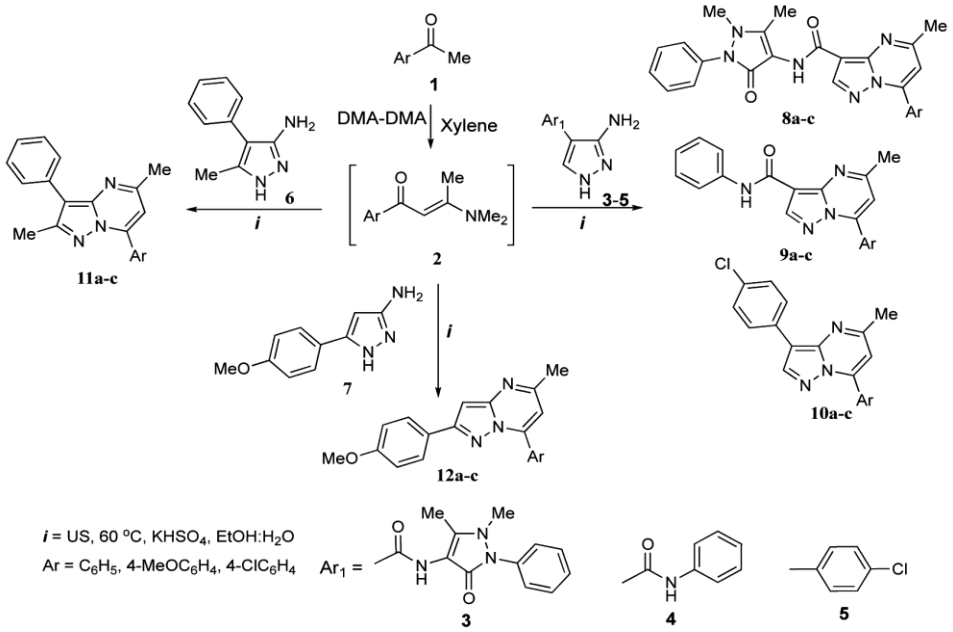

Scheme 1 — Synthesis of pyrazolo[1,5-*a*]pyrimidines (**8**-**12**)

precipitated product was collected by filtration, washed with water-ethanol (3×1 mL) and finally dried over calcium chloride in a desiccator to give practically pure products (**8**/**9**/**10**) in 96–97% yields. Further purification for analytical purposes was achieved by column chromatography (silica gel, 20% EtOAc–hexane).

***N*-(1,5-Dimethyl-3-oxo-2-phenyl-2,3-dihydro-*1H*-pyrazol-4-yl)-5-methyl-7-phenyl pyrazolo[1,5-*a*]pyrimidine-3-carboxamide, 8a**: Light brown solid (394 mg, 90% yield). m.p.211–212°C. IR (KBr): 1493 (C=C), 1558 (N–N), 1601 (CONH), 1668 (CO), 3478 (NH) cm^{-1}; ^1H NMR (300 MHz, $CDCl_3$): δ 2.40 (s, 3H, CH_3), 2.72 (s, 3H, CH_3), 3.11 (s, 3H, NCH_3), 6.93 (s, 1H, C_6–H), 7.42–7.51 (m, 5H, ArH), 7.53–7.59 (m, 3H, ArH), 7.98–8.03 (m, 2H, ArH), 8.67 (s, 1H, C_2–H), 9.52 (s, 1H, NH); ^{13}C NMR (75 MHz, $CDCl_3$): δ 13.04, 25.11, 36.76, 104.78, 109.70, 109.79, 123.99, 126.66, 128.95, 129.31, 129.57, 130.31, 131.66, 135.21, 146.66, 147.29, 147.59, 149.63, 161.17, 162.03, 162.16; HRMS [ESI] *m/z* Calcd for $C_{25}H_{22}N_6O_2$ $[MH]^+$: 439.1882. Found: 439.1886.

***N*-(1,5-Dimethyl-3-oxo-2-phenyl-2,3-dihydro-*1H*-pyrazol-4-yl)-7-(4-methoxyphenyl)-5-methylpyrazolo[1,5-*a*]pyrimidine-3-carboxamide, 8b**: Yellow solid (407 mg, 87% yield). m.p.213–214°C. IR (KBr): 1495 (C=C), 1551 (N–N), 1636 (CONH), 1666 (CO), 3297 (NH) cm^{-1}; ^1H NMR (300 MHz, $CDCl_3$): δ 2.40 (s, 3H, CH_3), 2.70 (s, 3H, CH_3), 3.10 (s, 3H, NCH_3), 3.89 (s, 3H, OCH_3), 6.90 (s, 1H, C_6–H), 7.06 (d, 2H, *J* = 9 Hz, ArH), 7.24–7.30 (m, 1H, ArH), 7.45–7.48 (m, 4H, ArH), 8.04 (d, 2H, *J* = 9 Hz, ArH), 8.66 (s, 1H, C_2–H), 9.55 (s, 1H, NH); ^{13}C NMR (75 MHz, $CDCl_3$): δ 13.05, 25.07, 36.78, 55.67, 104.53, 108.87, 109.80, 114.37, 122.34, 123.93, 126.59, 129.29, 131.40, 135.24, 146.47, 147.27, 147.45, 149.58, 161.24, 161.80, 162.15, 162.32; HRMS [ESI] *m/z* Calcd for $C_{26}H_{24}N_6O_3$ $[MH]^+$: 469.1988. Found: 469.2001.

7-(4-Chlorophenyl)-*N*-(1,5-dimethyl-3-oxo-2-phenyl-2,3-dihydro-*1H*-pyrazol-4-yl)-5-methylpyrazolo[1,5-*a*]pyrimidine-3-carboxamide, 8c: Light brown solid (434 mg, 92% yield). m.p.251–252°C. IR (KBr): 1491 (C=C), 1555 (N–N), 1654 (CONH), 1670 (CO), 3450 (NH) cm^{-1}; ^1H NMR (300 MHz, $CDCl_3$): δ 2.39 (s, 3H, CH_3), 2.72 (s, 3H, CH_3), 3.12 (s, 3H, NCH_3), 6.93 (s, 1H, C_6–H), 7.28–7.31 (m, 1H, ArH), 7.45–7.48 (m, 4H, ArH), 7.54 (d, 2H, *J* = 8.4 Hz, ArCl), 7.98 (d, 2H, *J* = 8.4 Hz, ArCl), 8.65 (s, 1H, C_2–H), 9.48 (s, 1H, NH); ^{13}C NMR (75 MHz, $CDCl_3$): δ 13.23, 24.70, 37.48, 104.61, 104.68, 109.20, 122.79, 124.84, 127.76, 128.16, 128.37, 129.62, 130.05, 131.89, 134.80, 146.08, 146.94, 146.98, 147.88, 160.91, 161.88; HRMS [ESI] *m/z* Calcd for $C_{25}H_{21}ClN_6O_2$ $[MH]^+$: 473.1493. Found: 473.1497.

5-Methyl-*N*,7-diphenylpyrazolo[1,5-*a*]pyrimidine-3-carboxamide, 9a: Yellow solid (302 mg, 92% yield). m.p.224°C. IR (KBr): 1475 (C=C), 1548 (N–N), 1618 (C=N), 1675 (CO), 3300 (NH) cm^{-1}; ^1H NMR (400 MHz, $CDCl_3$): δ 2.76 (s, 3H, CH_3), 6.94 (s, 1H, C_6–H), 7.08–7.11 (t, 1H, ArH), 7.34–7.38 (t, 2H, ArH), 7.57–7.58 (m, 3H, ArH), 7.75 (d, 2H, *J* = 8 Hz, ArH), 7.79–8.01 (m, 2H, ArH), 8.69 (s, 1H, C_2–H), 10.2 (s, 1H, NH); ^{13}C NMR (100 MHz, $CDCl_3$): δ 25.21, 105.21, 109.65, 111.04, 119.79, 123.72, 128.99, 129.12, 129.59, 130.16, 131.79, 139.04, 146.72, 147.79, 160.58, 161.60; MS [ESI] *m/z*: 329 $[MH]^+$; HRMS [ESI] *m/z* Calcd for $C_{20}H_{16}N_4O$ $[MH]^+$: 329.1402. Found: 329.1404.

7-(4-Methoxyphenyl)-5-methyl-*N*-phenylpyrazolo[1,5-*a*]pyrimidine-3-carboxamide, 9b: Yellow solid (326 mg, 91% yield). m.p.234°C. IR (KBr): 1456 (C=C), 1528 (N–N), 1612 (C=N), 1670 (CO), 3433 (NH) cm^{-1}; ^1H NMR (400 MHz, $CDCl_3$): δ 2.76 (s, 3H, CH_3), 3.90 (s, 3H, OCH_3), 6.93 (s, 1H, C_6–H), 7.07–7.10 (m, 3H, ArH), 7.35–7.39 (t, 2H, ArH), 7.77 (d, 2H, *J* = 8 Hz, ArH), 8.06 (d, 2H, *J* = 8 Hz, ArH), 8.70 (s, 1H, C_2–H), 10.27 (s, 1H, NH) ; ^{13}C NMR (100 MHz, $CDCl_3$): δ 25.21, 55.76, 105.08, 108.75, 114.48, 119.89, 122.28, 123.74, 129.18, 131.49, 139.16, 146.71, 146.96, 147.61, 160.76, 161.37, 162.49; MS [ESI] *m/z*: 359 $[MH]^+$; HRMS [ESI] *m/z* Calcd for $C_{21}H_{18}N_4O_2$ $[MH]^+$: 359.1507. Found: 359.1506.

7-(4-Chlorophenyl)-5-methyl-*N*-phenylpyrazolo[1,5-*a*]pyrimidine-3-carboxamide, 9c: Yellow solid (308 mg, 85% yield). m.p.205°C. IR (KBr): 1492 (C=C), 1554 (N–N), 1617 (C=N), 1666 (CO), 3325 (NH) cm^{-1}; ^1H NMR (300 MHz, $CDCl_3$): δ 2.74 (s, 3H, CH_3), 6.91 (s, 1H, C_6–H), 7.05–7.11 (m, 1H, ArH), 7.31–7.36 (t, 2H, ArH), 7.50–7.54 (m, 2H, ArCl), 7.69–7.72 (m, 2H, ArH), 7.95–7.99 (m, 2H, ArCl), 8.64 (s, 1H, C_2–H), 10.11 (s, 1H, NH) ; ^{13}C NMR (75 MHz, $CDCl_3$): δ 25.22, 105.34, 109.46, 119.77, 123.78, 128.47, 129.13, 129.28, 131.00,

138.12, 138.98, 146.51, 146.62, 146.68, 160.40, 161.64; MS [ESI] *m/z*: 363 $[MH]^+$; HRMS [ESI] *m/z* Calcd for $C_{20}H_{15}N_4ClO$ $[MH]^+$: 363.1012. Found: 363.1017.

3-(4-Chlorophenyl)-5-methyl-7-phenylpyrazolo[1,5-*a*]pyrimidine, 10a: Yellow solid (255 mg, 80% yield). m.p.148–149°C. IR (KBr): 1494 (C=C), 1559 (N–N), 1618 (C=N) cm^{-1}; ^1H NMR (300 MHz, $CDCl_3$): δ 2.68 (s, 3H, CH_3), 6.78 (s, 1H,C_6–H), 7.37–7.41 (m, 2H, ArCl), 7.53–7.58 (m, 3H, ArH), 7.96–7.98 (m, 2H, ArH), 8.01–8.06 (m, 2H, ArCl), 8.35 (s, 1H, C_2–H); ^{13}C NMR (75 MHz, $CDCl_3$): δ 25.23, 108.58, 109.02, 113.00, 127.60, 128.89, 128.97, 129.40, 131.16, 131.25, 131.69, 142.47, 145.96, 146.50, 159.51; MS [ESI] *m/z*: 320 $[MH]^+$; HRMS [ESI] *m/z* Calcd for $C_{19}H_{14}N_3Cl$ $[MH]^+$: 320.0954. Found: 320.0952.

3-(4-Chlorophenyl)-7-(4-methoxyphenyl)-5-methylpyrazolo[1,5-*a*]pyrimidine, 10b: Yellow solid (216 mg, 88% yield). m.p.184°C. IR (KBr): 1506 (C=C), 1561 (N–N), 1607 (C=N) cm^{-1}; ^1H NMR (300 MHz, $CDCl_3$): δ 2.66 (s, 3H, CH_3), 3.88 (s, 3H, OCH_3), 6.75 (s, 1H, C_6–H), 7.03–7.08 (m, 2H, $ArOCH_3$), 7.36–7.41 (m, 3H, $ArOCH_3$), 7.97–8.06 (m, 4H, ArCl), 8.35 (s, 1H, C_2–H); ^{13}C NMR (75 MHz, $CDCl_3$): δ 25.21, 55.67, 108.21, 108.33, 114.31, 123.35, 127.56, 128.95, 131.11, 131.28, 131.58, 142.33, 146.08, 146.23, 159.40, 161.91; MS [ESI] *m/z*: 349 $[M]^+$; HRMS [ESI] *m/z* Calcd for $C_{20}H_{16}N_3ClO$ $[MH]^+$: 350.1059. Found: 350.1056.

3,7-Bis(4-chlorophenyl)-5-methylpyrazolo[1,5-*a*]pyrimidine, 10c: Yellow solid (336 mg, 95% yield). m.p.211–212°C. IR (KBr): 1492 (C=C), 1525 (N–N), 1615 (C=N) cm^{-1}; ^1H NMR (300 MHz, $CDCl_3$): δ 2.70 (s, 3H, CH_3), 6.79 (s, 1H, C_6–H), 7.41 (d, 2H, *J* = 8.1 Hz, ArCl), 7.55 (d, 2H, *J* = 8.1 Hz, ArCl), 7.97 (d, 2H, *J* = 8.1 Hz, ArCl), 8.04 (d, 2H, *J* = 8.4 Hz, ArCl), 8.36 (s, 1H, C_2–H); ^{13}C NMR (75 MHz, $CDCl_3$): δ 24.68, 107.65, 108.50, 109.73, 126.21, 128.53, 129.43, 129.77, 130.69, 131.61, 140.86, 143.65, 145.04, 145.65, 159.59; MS [ESI] *m/z*: 355 $[MH]^+$; HRMS [ESI] *m/z* Calcd for $C_{19}H_{13}N_3Cl_2$ $[MH]^+$: 354.0564. Found: 354.0562.

Synthesis of 2-methyl-3-phenyl/2-(4-methoxyphenyl)-5-methyl-7-arylpyrazolo [1,5-*a*] pyrimidine-3-carboxamides 11a–c, 12a–c

To a solution of enaminone **2** (1 mmol)[51] and aminopyrazole (**6**/**7**) (1 mmol) in 2.5 mL EtOH was added $KHSO_4$ (2 mmol) dissolved in 2.5 mL of water in one lot and the resulting mixture was irradiated under the influence of ultrasound waves for 5–20 minutes resulting in the formation of a precipitated product (Scheme 1). After the completion of reaction (TLC), the precipitate was collected by filtration, washed repeatedly with ethanol–water (1:1) to ensure complete removal of acid and dried to give practically pure pyrazolopyrimidines (**11**/**12**) in 85–92% yields. Further, purification was achieved by column chromatography (silica gel, 20% EtOAc–hexane).

2,5-Dimethyl-3,7-diphenylpyrazolo[1,5-*a*]pyrimidine, 11a: Brown solid (260 mg, 87% yield). m.p.198°C. IR (KBr): 1475 (C=C), 1566 (N–N), 1617 (C=N) cm^{-1}; ^1H NMR (300 MHz,$CDCl_3$): δ 2.61 (s, 6H, $2CH_3$), 6.69 (s, 1H, C_6–H), 7.26–7.31 (t, 1H, ArH), 7.44–7.49 (t, 2H, ArH), 7.52–7.55 (m, 3H, ArH), 7.76 (d, 2H, *J* = 8.1 Hz, ArH), 8.02–8.05 (m, 2H, ArH); ^{13}C NMR (75 MHz, $CDCl_3$): δ 14.68, 25.11, 108.35, 108.53, 126.28, 128.64, 128.80, 129.18, 129.46, 130.98, 131.56, 132.95, 145.56, 147.22, 152.46, 158.87; MS [ESI] *m/z*: 300 $[MH]^+$; HRMS [ESI] *m/z* Calcd for $C_{20}H_{17}N_3$ $[MH]^+$: 300.1500. Found: 300.1496.

7-(4-Methoxyphenyl)-2,5-dimethyl-3-phenylpyrazolo[1,5-*a*]pyrimidine, 11b: Light brown solid (313 mg, 95% yield). m.p.186°C. IR (KBr): 1443 (C=C), 1556 (N–N), 1605 (C=N) cm^{-1}; ^1H NMR (300 MHz, $CDCl_3$): δ 2.60 (s, 3H, CH_3), 2.61 (s, 3H, CH_3), 3.88 (s, 3H, OCH_3), 6.67 (s, 1H, C_6–H), 7.05 (d, 2H, *J* = 9 Hz, $ArOCH_3$), 7.25–7.31 (m, 1H, ArH), 7.43–7.48 (t, 2H, ArH), 7.74–7.77 (m, 2H, ArH), 8.06 (d, 2H, *J* = 9 Hz, $ArOCH_3$); ^{13}C NMR (75 MHz, $CDCl_3$): δ 14.69, 25.10, 55.63, 107.54, 108.29, 114.23, 123.71, 126.19, 128.62, 129.15, 131.13, 133.06, 145.27, 147.32, 152.27, 158.77, 161.78; MS [ESI] *m/z*: 330 $[MH]^+$; HRMS [ESI] *m/z* Calcd for $C_{21}H_{19}N_3O$ $[MH]^+$: 330.1606. Found: 330.1602.

7-(4-Chlorophenyl)-2,5-dimethyl-3-phenylpyrazolo[1,5-*a*]pyrimidine, 11c: Light orange solid (319 mg, 96% yield). m.p.178°C. IR (KBr): 1489 (C=C), 1551 (N–N), 1611 (C=N) cm^{-1}; ^1H NMR (400 MHz, $CDCl_3$): δ 2.80 (s, 6H, CH_3), 6.70 (s, 1H, C_6–H), 7.30–7.33 (t, 1H, ArH), 7.47–7.50 (t, 2H, ArH), 7.54 (d, 2H, *J* = 8.4 Hz, ArCl), 7.76 (d, 2H, *J* = 8.0 Hz, ArH), 8.02 (d, 2H, *J* = 8.4 Hz, ArCl); ^{13}C NMR (100 MHz, $CDCl_3$): δ 14.67, 25.16, 108.20, 108.73, 126.41, 128.70, 129.15, 129.18, 129.89, 130.83, 132.77, 137.12, 144.33, 147.17, 152.58,

158.90; MS [ESI] *m/z*: 333 $[M]^+$; HRMS [ESI] *m/z* Calcd for $C_{20}H_{16}N_3Cl$ $[MH]^+$: 334.1110. Found: 334.1106.

2-(4-Methoxyphenyl)-5-methyl-7-phenylpyrazolo[1,5-*a*]pyrimidine, 12a: Yellow solid (302 mg, 96% yield). m.p.212°C. IR (KBr): 1459 (C=C), 1532 (N–N), 1611 (C=N) cm^{-1}; ^1H NMR (300 MHz, $CDCl_3$): δ 2.61 (s, 3H, CH_3), 3.83 (s, 3H, OCH_3), 6.72 (s, 1H,C_6–H), 6.83 (s, 1H, C_3–H), 6.93–6.97 (m, 2H, ArH), 7.52–7.57 (m, 4H, ArH), 7.89–7.94 (m, 2H, $ArOCH_3$), 8.10–8.16 (m, 2H, $ArOCH_3$) ; ^{13}C NMR (75 MHz, $CDCl_3$): δ 24.90, 55.50, 92.04, 108.00, 114.24, 126.03, 128.06, 128.64, 129.63, 131.01, 131.43, 145.79, 151.07, 155.81, 158.65, 160.43; MS [ESI] *m/z*: 316 $[MH]^+$; HRMS [ESI] *m/z* Calcd for $C_{20}H_{17}N_3O$ $[MH]^+$: 316.1449. Found: 316.1452.

2,7-Bis(4-methoxyphenyl)-5-methylpyrazolo[1,5-*a*]pyrimidine, 12b: Yellow amorphous (317 mg, 92% yield). m.p.156–157°C. IR (KBr): 1456 (C=C), 1507 (N–N), 1611 (C=N) cm^{-1}; ^1H NMR (300 MHz, $CDCl_3$): δ 2.59 (s, 3H, CH_3), 3.83 (s, 3H, OCH_3), 3.89 (s, 3H, OCH_3), 6.69 (s, 1H, C_6–H), 6.81 (s, 1H, C_3–H), 6.96 (d, 2H, *J* = 9 Hz, $ArOCH_3$), 7.05 (d, 2H, *J* = 9 Hz, $ArOCH_3$), 7.90–7.94 (m, 2H, $ArOCH_3$), 8.15–8.18 (m, 2H, $ArOCH_3$) ; ^{13}C NMR (75 MHz, $CDCl_3$): δ 24.88, 55.50, 55.62, 91.83, 107.13, 114.06, 114.22 , 123.58, 126.12, 128.03, 131.32, 145.48, 151.18, 155.38, 158.54, 160.39, 161.84; HRMS [ESI] *m/z* Calcd for $C_{21}H_{19}N_3O$ $[MH]^+$: 346.1555. Found: 346.1549.

7-(4-Chlorophenyl)-2-(4-methoxyphenyl)-5-methylpyrazolo[1,5-*a*]pyrimidine, 12c: Off white solid (321 mg, 92% yield). m.p.189–190°C. IR (KBr): 1456 (C=C), 1507 (N–N), 1612 (C=N) cm^{-1}; ^1H NMR (300 MHz, $CDCl_3$): δ 2.62 (s, 3H, CH_3), 3.85 (s, 3H, OCH_3), 6.71 (s, 1H, C_6–H), 6.84 (s, 1H, C_3–H), 6.97 (d, 2H, *J* = 7.8 Hz, $ArOCH_3$), 7.53 (d, 2H, *J* = 7.8 Hz, $ArOCH_3$), 7.90 (d, 2H, *J* = 7.5 Hz, ArCl), 8.10 (d, 2H, *J* = 7.5 Hz, ArCl); ^{13}C NMR (75 MHz, $CDCl_3$): δ 25.45, 56.24, 90.82, 108.64, 112.92, 125.39, 125.58, 126.69, 127.80, 129.56, 136.87, 144.30, 150.68, 155.64, 158.42, 160.21; HRMS [ESI] *m/z* Calcd for $C_{20}H_{16}ClN_3O$ $[MH]^+$: 350.1060. Found: 350.1052.

Docking: Materials and methods

Target protein preparation

In this study, two protein targets were considered against the 15 synthesized compounds to assess their antiviral and anticancer activities. The target protein structures of COVID-19 main protease and HER 2 Protein of Oral Cancer were retrieved from the Protein Data Bank with PDB IDs: 6LU7 and 3PP0 with resolutions 2.16 Å and 2.25 Å respectively for molecular docking studies (https://www.rcsb.org/)[54-57]. The pre-existing ligands N3 and 03Q were removed from the target protein using the UCSF CHIMERA software. The missing residues in the receptor PDB data were identified and reconstructed using the WHAT IF Interface, an internet server (https://swift.cmbi.umcn.nl/servers/html/index.html)[56,57]. The Energy Minimization of the receptors was also performed using the software UCSF CHIMERA (https://www.cgl.ucgf.edu/chimera/)[58,59].

Ligand preparation

A total of 15 ligands were synthesized and constructed in SDF (Structure Data File) file format which was then converted to .pdb format using Open Babel (https://sourceforge.net/projects/open) and viewed using the software UCSF CHIMERA[60]. These ligands were: ligand **8a**, ligand **8b**, ligand **8c**, ligand **9a**, ligand **9b**, ligand **9c**, ligand **10a**, ligand **10b**, ligand **10c**, ligand **11a**, ligand **11b**, ligand **11c**, ligand **12a**, ligand 1**2b** and ligand **12c**, respectively.

Energy Minimization

The ligands were subjected to energy minimization using UCSF CHIMERA software (https://www.cgl.ucsf.edu/chimera/) to avoid distorted geometries and obtain a low energy conformation. This energy minimization was achieved by completing 5000 Steepest Descent and 5000 Conjugate gradient cycles. During the minimization approach, the ligands were assigned Gasteiger-Hückel charges and AMBER ff14SB (Force fields). For the molecular docking study, the ligand structures were suitably optimized.

Catalytic Site Prediction

The CASTp (Computed Atlas of Surface Topography of Proteins) server (http://sts.bioe.uic.edu/castp/index.html?2cpk) was used to determine the binding site of the ligands in the target protein structures of COVID-19 major protease and HER 2 Protein of Oral Cancer[61]. The residues present in the catalytic/binding site of the target proteins are represented in Table 1.

Molecular Docking

A total of 30 molecular dockings were performed using Autodock Software (http://autodock.

Table 1 — Residues in the catalytic site of the target proteins

S. No.	Receptors	PDB IDs	Residues in the Active Site
1	Covid-19 Main protease	6LU7	THR24, THR25, THR26, LEU26, HIS41, THR45, SER46, MET49, PHE140, LEU141, ASP142, GLY143, SER144, CYS145, HIS163, MET165, GLU166, HIS172
2	HER 2 Protein of Oral Cancer	3PP0	LYS724, LEU726, GLY727, SER728, GLY729, ALA730, PHE731, VAL734, ALA751, LYS753, LEU755, ARG756, THR759, ALA763, GLU766, ILE767, GLU770, ALA771, MET774, SER783, ARG784, LEU785, VAL797, THR798, GLN799, LEU800, MET801, PRO802, TYR803, GLY804, CYS805, ASP808, HIS809, GLU812, ASP845, ARG849, ASN850, LEU852, THR862, ASP863, PHE864, G LY865, LEU866, ARG868

Table 2 — Grid box generated for the target proteins.

Target Proteins	Centre Grid Box			Spacing Angstroms	No. of Points in Dimensions		
	X	Y	Z		X	Y	Z
6LU7	–9.410	16.284	67.201	1.000 Å	24	24	24
3PP0	16.403	17.491	30.11				

scripps.edu/)[62,63]. To obtain the best conformational state of docking, the AutoGrid program was used to generate the grid box with points in X Y Z of 24×24×24 Å with a spacing of 1.000 Å for both the target proteins respectively (Table 2). Following the completion of molecular docking, the best conformation from each protein-ligand complexes were carefully analysed for their binding energies. The interaction between the ligand and the target protein of the docking complexes was investigated using the LigPlotv.1.4.5 program (https://www.ebi.ac.uk/thornton-srv/software/LigPlus/)[64,65].

Molecular dynamics simulation

The trajectory of the chosen complex (3pp0+**9c**) was analyzed using 1ns (nanosecond) of MD simulations with integrated docking and simulation solutions from SiBioLead (www.sibiolead.com). SiBioLead is a new approach in molecular dynamics automation with GROMACS software package under OPPLS/AA force field (https://www.gromacs.org/), (www.sibiolead.com)[66]. The systems were prepared for MD simulation using solvation within a water-filled 3D triclinic. The system was neutralized by introducing counter ions to balance the protein's charge. The steepest descent approach was used to minimize the system over a 50000-step period. The temperature was set to 300 K, and the systems were equilibrated for 100 ps (picoseconds) in the NVT ensemble (number of particles, volume, and temperature), followed by another 100 ps in the NPT ensemble. Following heating and equilibration, the systems underwent a 1ns production MD run in an NPT ensemble. SiBIOLEAD, a cloud-based technology uses the GROMACS tool to analyse MD trajectories. The compound trajectories of the complex (3pp0+**9c**) were investigated using Root Mean Square Deviation (RMSD), Root Mean Square Fluctuation (RMSF), and Radius of Gyration (RG).

Results and Discussion

Chemistry

Enaminones (**2**) required for the synthesis of the target pyrazolo[1,5-*a*]pyrimidines were obtained by refluxing compound **1** with *N*,*N*-dimethylacetamide dimethyl acetal (DMA-DMA) in xylene[51] and were used without purification.

Thus, when 3-aminopyrazole (**3**) was reacted with enaminone **2a** derived from acetophenone and $KHSO_4$ in aqueous medium in an ultrasonic bath, a product was isolated in 93% yield, the structure of which was established as *N*-(1,5-dimethyl-3-oxo-2-phenyl-2,3-dihydro-*1H*-pyrazol-4-yl)-5-methyl-7-phenylpyrazolo[1,5-*a*]pyrimidine-3-carboxamide (**8a**) on the basis of spectral and analytical data. The reaction conditions could well be applied for the reactions of aminopyrazole **3** with enaminones **2b**,**c** giving the desired products in 85–92% overall yields. The same methodology was applied for the reaction of aminopyrazoles **4**–**7** with enaminones (**2a**–**c**) giving the pyrazolopyrimidines **9**–**12** respectively in 83–95% overall yields (Scheme 1).

The structures of the synthesized compounds were confirmed by their spectral data (IR, ^{1}H NMR, ^{13}C NMR and MS spectroscopy). The IR spectra of compounds **8a–c** showed absorption bands at 3297–3478 cm^{-1} and 1666–1670 cm^{-1} due to N–H and C=O (amide group) stretching vibrations. In compound **9a–c**, the absorption band due to N–H and C=O

(amide group) appeared at 3300–3433 cm^{-1} and 1666–1675 cm^{-1} respectively. The ^1H NMR spectra of compounds **8a–c**, **9a–c** showed a sharp singlet for the methyl protons (at C–5), C_6–H and C_2–H protons at δ 2.68, 6.93, 8.67 respectively. Compounds **10a–c** gave singlet for the methyl protons (at C–5), C_6–H and C_2–H protons at δ 2.68, 6.8, 8.35 respectively. The signals due to aromatic protons resonated in their usual range.

In the case of compounds **11a–c**, the signals due to methyl protons at C–2 and C–5 resonated as sharp singlets at around δ 2.61. The signals due to C_6–H, appeared as a singlet at δ 6.69. Compounds **12a–c**, gave singlet at around δ 6.83 due to C_3–H proton, in addition to the singlet signal caused by the C_6–H proton at δ 6.71. Also, the methyl protons (at C–5) resonated as sharp singlet at about δ 2.60. For compounds **8b**, **9b**, **10b**, **11b**, **12b**, the methoxy proton resonated as singlet at about δ 3.88.

The ^{13}C NMR spectra for the synthesized compounds showed a distinct peak due to the methyl group at C–5 close to δ 25.0. In addition, compounds **8**, **9** gave a distinct signal for the amide carbon at δ 162.0. Mass spectra of the compounds further added to the confirmation of the structure.

X-ray Crystallography

N-(1,5-Dimethyl-3-oxo-2-phenyl-2,3-dihydro-*1H*-pyrazol-4-yl)-7-(4-methoxyphenyl)-5-methylpyrazolo[1,5-*a*]pyrimidine-3-carboxamide (**8b**) was selected as a model for X-ray crystallographic analysis. Slow crystallization of the compound was carried out using ethyl acetate whereby dull yellowish needle-like crystals were obtained. The crystallographic data for the structure were deposited to the Cambridge Crystallographic Data Center (CCDC no. 2312662). The single crystal X-ray diffraction studies reveal that the compound **8b** crystallized in the monoclinic space group $P2_1/n$ with a = 17.5775 (8) Å, b = 7.1707 (4) Å, c = 18.113 (1) Å, β = 91.449 (2)°, V = 2282.3 (2) $Å^3$ and Z = 4. The crystal structure of compound **8b** with atom labeling of the asymmetric unit is shown in Fig. 2. The crystal data and its refinement values are presented in Table 3.

Table 3 — Crystal data and structure refinement parameters of compound **8b**

Emperical Formula	$C_{26}H_{24}N_6O_3$
Formula Weight	468.52
Temperature (K)	296
Wavelength (Å)	0.71073
Crystal system, space group	Monoclinic, $P2_1/n$
a (Å)	17.5775 (8)
b (Å)	7.1707 (4)
c (Å)	18.113 (1)
β (°)	91.449 (2)
Volume ($Å^3$)	2282.3 (2)
Z	4
Radiation	Mo Kα
Absorption coefficient (mm^{-1})	0.09
F_{000}	984.654
θ range for data collection	3.1-28.3°
Index ranges	$-20 \le h \le 23$, $-9 \le k \le 9$, $-24 \le l \le 24$
Reflections collected	49592
Independent reflections	5730
R_{int}	0.086
Data/restraints/parameters	5730/0/324
Goodness-of-fit on F^2	1.09
Final [$I > 2\sigma(I)$]	49592, 5730,3916
R indices (all data)	0.062
Largest diff. peak and hole	0.61, –0.60
CCDC No.	2312662

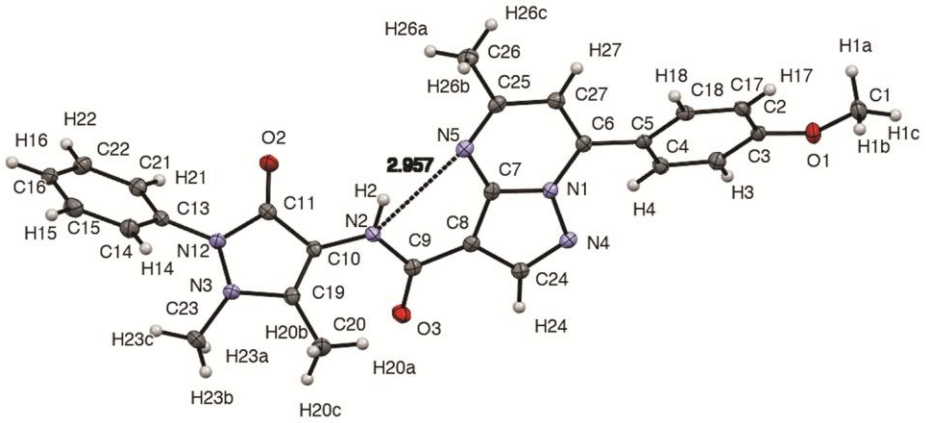

Fig. 2 — X-ray structure of compound **8b**

Some selected bond angles and bond lengths are mentioned in Table 4. The substituents attached to the pyrazolopyrimidine ring at C_3, C_5 and C_7 are at a distance of 1.463 (3) 1.494 (3) 1.467 (3) Å *i.e*., C8–C9, C25–C26, C6–C5 respectively. The pyrazolo[1,5-*a*] pyrimidine ring is found to be planar and the bond angles and bond lengths occur in their usual range [29] with the C–C bond distances ranging between 1.372–1.414 Å. The bond distances of N1–N4, N5–C25, C6–N1 are 1.378 (2), 1.328 (3), 1.375 (3) Å, respectively. The phenyl group at C6 appeared slightly tilted from the planarity of the pyrazolopyrimidine ring with torsional angle of N1–C6–C5–C4 and N1–C6–C5–C18 at 36.7 (2) and -145.88 (18) respectively. The perspective packing crystal structure for the compound can be viewed in Fig. 3 wherein each unit of the compound are arranged in an anti-parallel fashion. There is no significant intermolecular bonding besides vander waals interaction being responsible for the stability of the supramolecular framework. Compound **8b** showed the existence of weak intramolecular interaction among N2—N5 with interatomic distance of 2.957 Å. The bond length of O2–C11 and O3–C9 are 1.228 (2) and 1.226 (2) Å respectively as expected for a carbonyl bond. Due to steric hindrance between the N3-methyl and C19-methyl, the methyl group at N3 are slightly out of the plane of the antipyrine ring and the torsional angle of C23–N3–C19–C20 was -48.70 Å. The plane of the pyrazolone ring (C10 to C19) of the antipyrinyl group showed slight deviation from the plane of the amido (-N2H2–C9O3-) with torsional angles -130.44 and 52.99 for C11–C10–N2–C9 and C19–C10–N2–C9 respectively[67].

Table 4 — Selected bond lengths and bond angles of compound **8b**

Bond Lengths	Distance	Bond Angles	(°)
O1—C1	1.430 (3)	C2—O1—C1	117.98 (17)
O1—C2	1.361 (2)	C6—N1—N4	126.34 (16)
C10—C19	1.352 (3)	C7—N1—N4	112.28 (16)
C11—N12	1.390 (3)	C7—N1—C6	121.39 (17)
O2—C11	1.228 (2)	C10—N2—C9	123.28 (18)
N12—C13	1.416 (3)	C23—N3—N12	113.57 (17)
O3—C9	1.226 (2)	C22—C16—C15	119.6 (2)
C13—C14	1.392 (3)	C18—C17—C2	119.27 (19)
N1—N4	1.378 (2)	C17—C18—C5	121.6 (2)
C13—C21	1.386 (3)	C10—C19—N3	109.45 (18)
N1—C6	1.375 (3)	C3—C2—O1	115.44 (19)
N5–C25	1.328 (3)	C17—C18—C5	121.6 (2)
N1—C7	1.386 (2)	C4—C3—C2	120.3 (2)
N2—C9	1.367 (3)	C18—C5—C4	118.28 (18)
N2—C10	1.405 (3)	C27—C6—N1	114.99 (18)
C8–C9	1.463 (3)	C21—C13—C14	120.62 (19)
C6–C5	1.467 (3)	C27—C25—N5	122.24 (19)
C25–C26	1.494 (3)	C8—C24—N4	114.25 (18)

Molecular docking analysis

Molecular docking was conducted to analyse the binding mode interaction between the synthesized

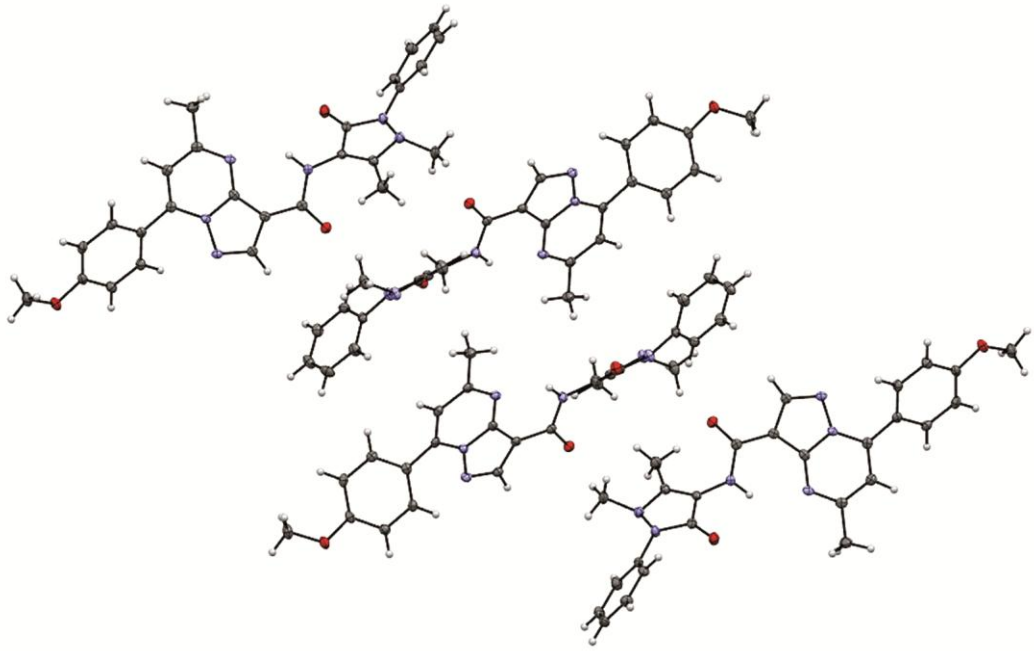

Fig. 3 — Packing structure of **8b**

compounds and the target receptor at the catalytic region. The binding energy of the ligands (**8a-c**, **9a-c**, **10a-c**, **11a-c**, and **12a-c**), when docked against the target protein Covid-19 Main protease (PDB ID 6LU7), was found to be -4.64, -3.92, -4.54, -4.63, -5.12, -4.98, -5.63, -5.65, -5.05, -5.75, -5.14, -6.04, -5.68, -4.20, and 4.42 kcal/mol, respectively as depicted in Table 5. Several studies provide valuable insights into how docking studies on SARS individually contribute to drug discovery efforts, targeting viral infections and cancer[68,69]. A recent molecular docking study revealed that flavolignans show high binding affinities against SARS-CoV-2 Mpro which can be used to design effective antiviral drug candidates against the SARS-CoV-2[70]. In the present study, the binding energy of the ligands, when docked against the HER 2 Protein of Oral Cancer (PDB ID 3PP0), was found to be -6.92, -7.91, -8.67, -9.02, -9.43, -9.43, -8.20, -8.63, -8.69, -8.25, -7.83, -8.70, -7.95, -7.82, and 8.46 kcal/mol, respectively as depicted in Table 6. The molecular docking study showed that all 15 synthesized compounds in complex

Table 5 — Molecular Docking of the synthesized compounds against the target protein COVID-19 Protease (PDB ID 6LU7)

S. No	Ligands	Target Protein	Binding Energy (kcal/mol)	Inhibition Constant (μM)	Hydrogen Bonds
1.	**8a**	*COVID-19 Protease* (PDB ID 6LU7)	–4.64	399.03	(No bond)
2.	**8b**		–3.92	1.33	GLN107(A), ARG105(A)
3.	**8c**		–4.54	472.41	(No bond)
4.	**9a**		4.63	401.5	(No bond)
5.	**9b**		–5.12	178.0	SER158(A)
6.	**9c**		–4.98	222.51	GLY138(A)
7.	**10a**		–5.63	74.64	(No bond)
8.	**10b**		–5.65	71.91	THR111(A)
9.	**10c**		–5.05	199.83	GLN107(A)
10.	**11a**		–5.75	61.37	(No bond)
11.	**11b**		–5.14	170.82	(No bond)
12.	**11c**		–6.04	37.42	(No bond)
13.	**12a**		–5.68	68.21	GLN110(A)
14.	**12b**		–4.20	840.95	PHE294(A), THR292(A)
15.	**12c**		–4.42	574.75	(No bond)
16.	Azithromycin	Control	–0.4	505.84	(No bond)

Table 6 — Molecular Docking of the synthesized compounds against the target protein HER 2 Protein of Oral Cancer (PDB ID 3PP0)

S. No	Ligands	Target Protein	Binding Energy (kcal/mol)	Inhibition Constant (μM)	Interacting Residues
1.	**8a**	*HER 2 Protein of Oral Cancer* (PDB ID 3PP0)	–6.92	8.41	No bond
2.	**8b**		–7.91	1.58	No bond
3.	**8c**		–8.67	441.47	No bond
4.	**9a**		–9.02	246.25	THR862(A)
5.	**9b**		–9.43	123.20	THR862(A)
6.	**9c**		–9.43	122.64	THR862(A)
7.	**10a**		–8.20	970.32	ASP863(A)
8.	**10b**		–8.63	473.60	No bond
9.	**10c**		–8.69	427.49	No bond
10.	**11a**		–8.25	894.66	No bond
11.	**11b**		–7.83	1.82	No bond
12.	**11c**		–8.70	419.50	No bond
13.	**12a**		–7.95	1.50	No bond
14.	**12b**		–7.82	1.87	No bond
15.	**12c**		–8.46	627.72	No bond
16.	Fluorouracil	Control	–3.43	3.05	THR862(A), SER783(A), ASP863(A)

with the target protein Covid-19 Main protease (PDB ID 6LU7) had poor binding energies ranging from -3.92 to -6.04 kcal/mol. Unlike, the molecular docking study of the compounds in the complex with the HER 2 Protein of Oral Cancer (PDB ID 3PP0) had good binding energies ranging from -6.92 to -9.43 kcal/mol. This showed that the synthesized compounds were more compatible with the HER 2 Protein of Oral Cancer (PDB ID 3PP0) in comparison to the target protein Covid-19 Main protease (PDB ID 6LU7). In comparison to the synthesized compounds, the resulting binding energy level of the drug Azithromycin against Covid-19 Main protease (PDB ID 6LU7) was found to be -0.4 kcal/mol and the drug Fluorouracil against HER 2 Protein of Oral Cancer (PDB ID 3PP0) was found to be -3.43 kcal/mol respectively. This depicted that the binding energy of the synthesized compounds against the target proteins was better and more compatible than the commercially available drugs.

Along with the binding energy, the inhibition constant of the ligands against the target protein Covid-19 Main protease (PDB ID 6LU7) was also calculated and found to be 399.03, 1.33, 472.41, 401.50, 178.0, 222.51, 74.64, 71.91, 199.83, 61.37, 170.82, 37.42, 68.21, 840.95, and 574.75 μM, respectively as depicted in Table 5. The inhibition constant of the ligands against the HER 2 Protein of Oral Cancer (PDB ID 3PP0) was found to be 1.58, 441.47, 246.25, 123.20, 122.64, 970.32, 437.60, 427.49, 894.66, 1.82, 419.50, 1.50, 1.87, and 627.72 μM, respectively as depicted in Table 6. The lower the inhibition constant (μM), the stronger the binding affinity, requiring less medicine to effectively block the activity of the target receptor. The binding energies, inhibition constants, and the bond residues of all the protein-receptor complexes are depicted in Table 5 and Table 6.

The docking complexes with the highest binding energies observed were the 6LU7+**11c** and 3PP0+**9c**, respectively. The molecular docking study of all the 15 synthesized compounds along with the reference drugs was conducted using the site-specific approach (Table 5, Table 6). To validate our docking scores, blind docking was also performed for the two complexes with the highest binding energies (6LU7+**11c** and 3PP0+**9c**) respectively. It was found that the binding score of the blind docking for the complex 6LU7+**11c** and 3PP0+**9c** were 203.5 and 219.47 kcal/mol respectively. This showed that the site-specific approach demonstrated better binding affinity in comparison to the blind docking score. The docking complexes with the highest binding energies against their respective target proteins have been represented in 3-dimensional in Fig. 4.

The interaction of all the 15 synthesized ligands with the target protein Covid-19 Main protease (PDB ID 6LU7) and the HER 2 Protein of Oral Cancer (PDB ID 3PP0) was evaluated using the LigPlot and the Chimera Software as depicted in Table **S1** (supplemental file). It was observed that the binding pattern of complexes 6LU7+**8a**, 6LU7+**8c**, 6LU7+**9a**, 6LU7+**10a**, 6LU7+**11a**, 6LU7+**11b**, 6LU7+**11c**, 6LU7+**12c**, 3PP0+**8a**, 3PP0+**8b**, 3PP0+**8c**, 3PP0+**10b**, 3PP0+**10c**, 3PP0+**11a**, 3PP0+**11b**, 3PP0+**11c**, 3PP0+**12a**, 3PP0+**12b**, 3PP0+**12c** have no hydrogen bonds. However, the binding pattern of complex 6LU7+**8b** showed two hydrogen bonds of length 2.95 Å at position 107 with Glutamine and 3.07 Å at position 105 with Arginine of chain A. Complex 6LU7+**9b** had one hydrogen bond of length 3.01 Å at position 158 with Serine of chain A. Likewise, the binding pattern of complex 6LU7+**9c** had one hydrogen bond of length 2.88 Å with Glycine at position 138 of chain A. The binding pattern of complex 6LU7+**10b** displayed one hydrogen bond of

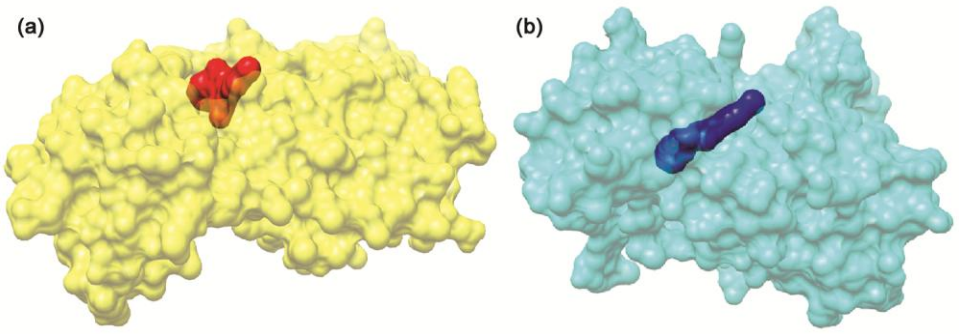

Fig. 4 — 3D Representation of the docking complexes with the highest binding energy values from Tables 5 and 6. **(A)** 6LU7+**11c** and **(B)** 3PP0+**9c**

length 3.33 Å at position 111 with Threonine of chain A. Similarly, the binding pattern of complex 6LU7+**10c** exhibited one hydrogen bond of length 3.17 Å at position 107 with Glutamine of chain A. The binding pattern of complex 6LU7+**12a** showed one hydrogen bond of length 2.92 Å at position 110 with Glutamine of chain A and that of complex 6LU7+**12b** presented two hydrogen bonds of length 3.23 Å at position 294 with Phenylalanine and 3.33 Å at position 292 with Threonine of chain A. The binding pattern of complex 3PP0+**9a** had one hydrogen bond of length 2.96 Å at position 862 with Threonine of chain A. In like manner, the binding pattern of complex 3PP0+**9b** revealed one hydrogen bond of length 2.85 Å at position 862 with Threonine of chain A while the binding pattern of complex 3PP0+**9c** had one hydrogen bond of length 2.80 Å at position 862 with Threonine of chain A. The binding pattern of complex 3PP0+**10a** exhibited one hydrogen bond of length 3.12 Å at position 863 with Asparagine of chain A. Overall, the most common residue involved in hydrogen bonds among all the complexes observed was the Threonine (THR) amino acid of the target proteins.

From the *in-silico* studies, the ligands **8c, 9a, 9b, 9c, 10a, 10b, 10c, 11a, 11b, 11c, 12a, and 12c** were identified as promising drug candidates against COVID-19 main protease and HER 2 Protein of Oral Cancer. The molecular docking study revealed that the synthesized compounds had poor binding energies in complex with the target protein Covid-19 Main protease (PDB ID 6LU7) ranging from -3.92 to -6.04 kcal/mol. In contrast, the compounds exhibited good binding energies ranging from -6.92 to -9.43 kcal/mol with the HER 2 Protein of Oral Cancer (PDB ID 3PP0), indicating better compatibility with the latter.

Molecular dynamic simulation

After the molecular docking, one of the probable ligand candidates (**9c**) in the complex with the 3pp0 receptor in this study was subjected to Molecular Dynamics Simulations to examine the stability of the complex. Molecular dynamics (MD) simulations are the most essential technique for structure-based drug design[71,72]. This computational tool uses Newton's second law of motion [F=ma][73] to analyse the physical movement of atoms and molecules. Atoms and molecules may only interact for a set amount of time, providing a dynamic perspective. Internal protein mobility is provided by increasing and then decreasing the system's temperature over a very brief period. This condition aids in the removal or modification of faulty bonds between peptides and residues, resulting in the protein's most stable and energy-efficient structure by computing alternative trajectories of the same conformation.

In this study, the compound **9c** in complex with the target receptor 3pp0 which demonstrated both good antiviral and anticancer activity with a high binding energy score was selected for Molecular Dynamics Simulations. This was done to demonstrate the flexibility and overall stability of the selected docked complex at 1ns using a cloud-based technology tool SiBioLead (www.sibiolead.com), which is a new approach in molecular dynamics automation with the GROMACS software package. Overall, the MD Simulation analysis revealed the stability of the potential ligand candidate (**9c**).

Root Mean Square Deviation (RMSD)

Root mean square deviation (RMSD) plots for the selected compound **9c** with 3pp0 receptor reflected the stability of the structures at 300 K for 1 ns. Fig. 5(a) reveals fluctuation of the protein from

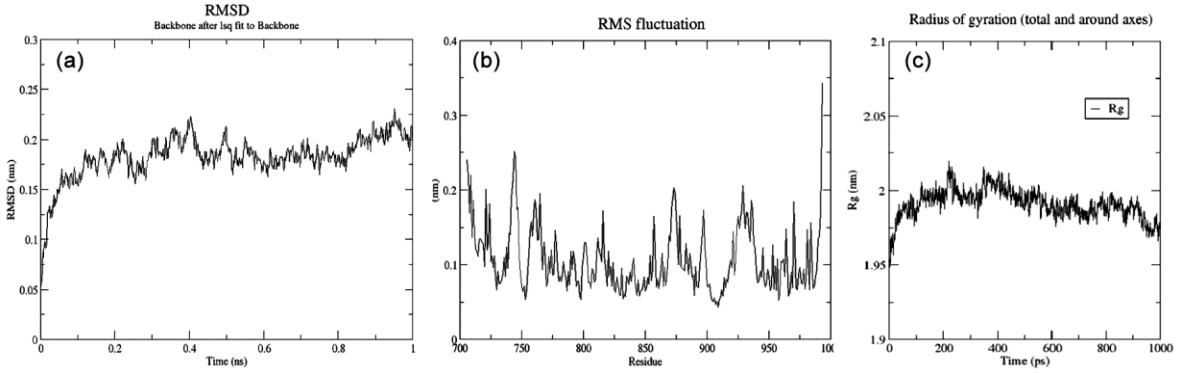

Fig. 5 — (a) RMSD along MD trajectories for compound **9c** with the receptor 3pp0 during the entire simulation. (b) RMSF along MD trajectories for compound **9c** with the receptor 3pp0 during the entire simulation. (c) Radius of Gyration obtained through MD Analysis of 3pp0+**9c**

0.2 nm to 0.4 nm within 1ns before reaching equilibrium. Slight fluctuations were observed before reaching equilibrium.

Root Mean Square Fluctuation (RMSF)

Root mean square Fluctuation (RMSF) plots for the selected compound **9c** with 3pp0 receptor reflected the flexibility of the structures at 300 K for 1 ns. Fig. 5(b) reveals the flexibility change of the ligands at 750 and within nearby 900 to 950 during the simulation. Higher fluctuations of the ligand were observed throughout the simulation depicting more flexibility.

Radius of Gyration (RG)

Radius of gyration (RG) plots for the selected compound **9c** with the receptor 3pp0 reflected the Compactness of the structures at 300 K for 1 ns. This reveals any conformational changes in protein and predicts the compactness of the protein which in turn reflects its stability. Fig. 5(c) reveals the compactness of the 3pp0 receptor with ligand **9c**.

Conclusion

We have devised an efficient, straightforward, and environment-friendly approach for the synthesis of pyrazolo[1,5-*a*]pyrimidine derivatives using a variety of 3-aminopyrazoles and acylated active proton compounds in the presence of $KHSO_4$ in aqueous medium. The chosen synthetic strategy has proven remarkably efficient in the annulation of pyrazolo[1,5-*a*]pyrimidines with the introduction of methyl group at position 5. This strategy not only delineates a simplified process but also leads to expanding their molecular diversity. Employing ultrasound tools additionally proved to be quite efficient in reducing energy consumption and concurrently maximizing yields of pure products. It also leads to the accelerated reaction times with a heightened cost-effectiveness.

The *in silico* investigations revealed the ligands **8c**, **9a**, **9b**, **9c**, **10a**, **10b**, **10c**, **11a**, **11b**, **11c**, **12a**, and **12c** as effective inhibitors, demonstrating potential as agents against both viral infections and cancer. The synthesized compounds demonstrated greater compatibility with the HER 2 Protein of Oral Cancer (PDB ID 3PP0) than with the Covid-19 main protease protein (PDB ID 6LU7). Compound **9c** in complex with the target receptor 3pp0, demonstrated both good antiviral and anticancer activity with a high binding energy score. The Molecular Dynamics Simulation investigation into the complex 3pp0+**9c** employing RMSD revealed its stability over a 1 ns period. Complementing this, MD analysis with RMSF and RG units shed light on the flexibility and compactness of the complex, thereby boosting the stability of the potential candidate **9c**. The *in-silico* screening of the synthesized ligands would therefore assist in identifying possible drug candidates. Further studies on these molecules are in progress in our laboratory.

Acknowledgements

Authors wish to thank, Rev. Fr. Dr. Stephen Mavely Founder Vice Chancellor, Rev. Fr. Dr. Jose Palely, Vice Chancellor, Rev. Fr. Joseph Nellanatt, Pro-Vice Chancellor, Assam Don Bosco University for providing infrastructure for the execution of this work. Authors also wish to express their gratitude to IIT, Guwahati, Tezpur University, Tezpur, SAIF-NEHU, Shillong and SAIF-CDRI, Lucknow for spectral and analytical data and X-ray crystallographic studies. Our thanks are also due to ICAR-Umiam (Meghalaya), DBT-NER-BPMC. Special thanks to our colleagues Labet Bankynmaw Marpna and Tara Rangrime. A. Sangma for their valuable inputs while writing the manuscript and also for their unconstrained help.

Supplementary Information

Supplementary information is available in the website http://nopr.niscpr.res.in/handle/123456789/58776.

Funding

This research did not receive any specific grant from funding agencies in the public, commercial, or not-for-profit sectors.

[This article is a part of the thesis uploaded at shodhganga@inflibnet]

Declaration of Competing Interest

The authors declare that they have no known competing financial interests or personal relationships that could have appeared to influence the work reported in this paper.

References

1 Hossan A, Alrefaei A F, Katouah H A, Bayazeed A, Asghar B H, Shaaban F, El-Metwaly & N M, *J Saudi Chem Soc*, 27 (2023) 101599.

2 Abdallah A E M & Elgemeie G H, *Med Chem*, 18 (2022) 926.

3 Atta K F M, Ibrahim T M, Farahat O O M, Al-Shargabi T Q, Marei M G, Bekhit A A & Ashry El S H, *Fut Med Chem*, 9 (2017) 1913.

4 Asati V, Anant A, Patel P, Kaur K & Gupta G D, *Eur J Med Chem*, 225 (2021) 113781.
5 Cherukupalli S, Karpoormath R, Chandrasekaran B, Hampannavar G A, Thapliyal N & Palakollu V N, *Eur J Med Chem*, 126 (2017) 298.
6 Meng H, Liu Y & Lai L, *Acc Chem Res*, 48 (2015) 2242.
7 Ivachtchenko A V, Golovina E S, Kadieva M G, Kysil V M, Mitkin O D, Tkachenko S E & Okun I M, *J Med Chem*, 54 (2011) 8161.
8 Abdelhamid A O, Abdelall E K, Abdel-Riheem N A & Ahmed S A, *Phosphorus, Sulfur, Silicon, Related Elements*, 185 (2010) 709.
9 Kaping S, Kalita U, Sunn M, Singha L I & Vishwakarma J N, *Monatsh Chem*, 147 (2016) 1257.
10 Abdelgawad M A, Elkanzi N A A, Musa A, Ghoneim M M, Ahmad W, Elmowafy M, Ali A M A, Abdelazeem A H, Bukhari S N A, El-Sherbiny M, Abourehab M A S & Bakr B, *Arabian J Chem*, 15 (2022) 104015.
11 Attia M H, Elrazaz E Z, El-Emam S Z, Taher A T, Abdel-Aziz H A & Abouzid K A M, *Bioorg Chem*, 94 (2020) 103458.
12 Gregg B T, Tymoshenko D O, Razzano D A & Johnson M R, *J Comb Chem*, 9 (2007) 507.
13 Li Y-Z, Wang G-D, Yang H-Y, Hou L, Wang Y-Y & Zhu Z, *Chem Eur J*, 26 (2020) 16402.
14 Falcó J L, Piqué M, González M, Buira I, Méndez E, Terencio J, Pérez C, Príncep M, Palomer A & Guglietta A, *Eur J Med Chem*, 41 (2006) 985.
15 Parry D, Guzi T, Shanahan F, Davis N, Prabhavalkar D, Wiswell D, Seghezzi W, Paruch K, Dwyer M P, Doll R, Nomeir A, Windsor W, Fischmann T, Wang Y, Oft M, Chen T, Kirschmeier P & Lees E M, *Mol Canc Ther*, 9 (2010) 2344.
16 Hao J, Ho J N, Lewis J A, Karim K A, Daniels R N, Gentry P R, Hopkins C R, Lindsley C W & Hong C C, *ACS Chem Biol*, 5 (2010) 245.
17 Lippa A, Czobor P, Stark J, Beer B, Kostakis E, Gravielle M, Bandyopadhyay S, Russek S J, Gibbs T T, Farb D H & Skolnick P, *PNAS USA*, 102 (2005) 7380.
18 Watanabe Y S, Yasuda Y, Kojima Y, Okada S, Motoyama T, Takahashi R & Oka M, *J Enzym Inhib Med Chem*, 30 (2015) 981.
19 a) Hassan A Y, Saleh N M, Kadh M S, Abou-Amra E S, *J Heterocycl Chem*, 57 (2020) 2704.; b) Dunn P J, Galvin S & Hettenbach K, *Green Chem*, 6 (2004) 43.
20 Dunn P J, Galvin S & Hettenbach K, *Green Chem*, 6 (2004) 43.
21 Karimzadeh M, Manouchehri N, Saberi D & Niknam K, *Struc Chem*, 29 (2018) 383.
22 Sivaiah G, Raveesha R, Prasad S B B, Kumar K Y, Raghu M S, Alharethy F, Prashanth M K & Jeon B –H, *J Mol Struc*, 1289 (2023) 135877.
23 Ismail N S M, Ali G M E, Ibrahim D A & Elmetwali A M, *Fut J Pharm Sci*, 2 (2016) 60.
24 Stypik M, Zagozda M, Michałek S, Dymek B, Zdżalik-Bielecka D, Dziachan M, Orłowska N, Gunerka P, Turowski P, Hucz-Kalitowska J, Stanczak A, Stańczak P, Mulewski K, Smuga D, Stefaniak F, Gurba-Bryskiewicz L, Leniak A, Ochal Z, Mach M, Dzwonek K, Lamparska-Przybysz M, Dubiel K & Wieczorak M, *Pharmaceuticals*, 15 (2022) 949.
25 Peytam F, Adib M, Shourgeshty R, Firoozpour L, Rahmanian-Jazi M, Jahani M, Moghimi S, Divsalar K, Faramarzi M A, Mojtabavi S, Safari F, Mahdavi M & Foroumadi A, *Sci Rep*, 10 (2020) 2595.
26 Mohamed M S, Saad Z A & Metwally N H, *Chem Sel*, 8 (2023) e202301286.
27 Arias-Gómez A, Godoy A & Portilla J, *Molecules*, 26 (2021) 2708.
28 Tigreros A, Macías M & Portilla J, *Dyes Pigment*, 184 (2021) 108730.
29 Portilla J, Quiroga J, Cobo J, Low J N & Glidewell C, *Acta Cryst*, C62 (2006) 186.
30 Mekky A E M & Sanad S M H, *Chem Sel*, 8 (2023) e202300487.
31 Williamson D S, Parratt M J, Bower J F, Moore J D, Richardson C M, Dokurno P, Howes R, Jackson P S, Lockie A M, Murray J B, Nunns C L, Powles J, Robertson A, Surgenor A E & Torrance C J, *Bioorg Med Chem Lett*, 15 (2005) 863.
32 Paruch K, Dwyer M P, Alvarez C, Brown C, Chan T-Y, Doll R J, Keertikar K, Knutson C, McKittrick B, Rivera J, Rossman R, Tucker G, Fischmann T O, Hruza A, Madison V, Nomeir A A, Wang Y, Lees E, Parry D, Sgambellone N, Seghezzi W, Schultz L, Shanahan F, Wiswell D, Xu X, Zhou O, James R A, Paradkar V M, Park H, Rokosz L R, Stauffer T M & Guzi T J, *Bioorg Med Chem Lett*, 17 (2007) 6220.
33 Patnaik S, Zheng W, Choi J H, Motabar O, Southall N, Westbroek W, Lea W A, Velayati A, Goldin E, Sidransky E, Leister W & Marugan J J, *J Med Chem*, 55 (2012) 5734.
34 Mikami S, Sasaki S, Asano Y, Ujikawa O, Fukumoto S, Nakashima K, Oki H, Kamiguchi N, Imada H, Iwashita, H & Taniguchi T, *J Med Chem*, 60 (2017) 7658.
35 Kaping, S, Helissey, P & Vishwakarma J N, *Eur J Med Chem*, 11 (2020) 179.
36 Kaping S, Sunn, M, Singha, L I & Vishwakarma J N, *Eur J Med Chem*, 11 (2020) 68.
37 Kaping S, Sympli H D, Marpna L B & Vishwakarma J N, *J Mol Struc*, 1288 (2023) 135766.
38 Kaping S, Boiss I, Singha L I, Helissey P & Vishwakarma J N, *Mol Divers*, 20 (2016) 379.
39 Marjani A P, Khalafy J, Salami F & Ezati M, *Arkivoc*, V (2015) 277.
40 Houas N, Kitouni S, Chafai N, Ghedjati S, Djenane M & Tounsi A, *J Mol Struc*, 1284 (2023) 135356.
41 Hilgenfeld R, *FEBS J*, 281 (2014) 4085.
42 Zhang L, Lin D, Sun X, Curth U, Drosten C, Sauerhering L, Becker S, Rox K & Hilgenfeld R, *Science*, 368 (2020) 409.
43 Issa S S, Sokornova S V, Zhidkin R R & Matveeva T V, *Plants* 11 (2022) 1862.
44 Mengist H M, Dilnessa T & Jin T, *Front Chem*, 9 (2021) 622898.
45 Gadewar M & Lal B, *Int J Appl Pharm*, 14 (2022) 100.
46 Riese D J & Stern D F, *Bio Essays*, 20 (1998) 41.
47 Olayioye M A, *Breast Can Res*, 3 (2001) 385.
48 Neve R M, Lane H A & Hynes N E, *Ann Onco*l, 12 (2001) S9.
49 Ménard S, Pupa S M, Campiglio M & Tagliabue E, *Oncogene*, 22 (2003) 6570.
50 Pollock N I & Grandis J R, *Clin Cancer Res*, 21 (2015) 526.

51 Kalita U, Kaping S, Nongkynrih R, Sunn M, Boiss I, Singha L I & Vishwakarma J N, *Med Chem Res*, 24 (2015) 32.
52 Sheldrick G M, *Acta Cryst*, 71 (2015) 3.
53 Dolomanov O V, Bourhis L J, Gildea R J, Howard J A & Puschmann H, *J Appl Cryst*, 42, (2009) 339.
54 RCSB Protein Data Bank, RCSB PDB: Homepage https://www.rcsb.org/ (accessed Jan 30, 2021).
55 Alisha K & Tripti S, *Res J Pharm Tech*, 14 (2021) 3757.
56 Mukhopadhyay S & Sarkar A, *Res Square*, (2021) 1, (https://doi.org/10.21203/rs.3.rs-618799/v1).
57 Arya H, Coumar M S, (Academic Press) 2021, p. 31.
58 Zhang S, Krumberger M, Morris M A, Parrocha C M, Kreutzer A G & Nowick J S, *Eur J Med Chem*, 218 (2021) 113390.
59 Pettersen E F, Goddard T D, Huang C C, Meng E C, Couch G S, Croll T I, Morris J H & Ferrin T E, *Protein Sci*, 30 (2021) 70.
60 Kim S, Chen J, Cheng T, Gindulyte A, He J, He S, Li Q, Shoemaker B A, Thiessen P A, Yu B, Zaslavsky L, Zhang J & Bolton E E, *Nucleic Acids Res*, 49 (2021) D1380.
61 Tian W, Chen C, Lei X, Zhao J & Liang J, *Nucleic acids Res*, 46 (2018) W363.
62 Meng X, Zhang H, Mezei M & Cui M, *Curr Comput Aided Drug Des*, 7 (2011) 146.
63 Ghersi D & Sanchez R, *Proteins*, 74 (2009) 417.
64 Souza P F, Lopes F E, Amaral J L, Freitas C D & Oliveira J T, *Int J Biol Macromol*, 164 (2020) 66.
65 Laskowski R A & Swindells M B, *J Chem Inf Model*, 51 (2011) 2778.
66 Spoel V D, Lindah E, Hess B, Groenhof G, Mark A E & Berendsen H J, *J Comp Chem*, 26 (2005) 1701.
67 Alam,M S & Lee D-U, *EXCLI*, 15 (2016) 614.
68 Peele K A, Durthi C P, Srihansa T, Krupanidhi S, Ayyagari V S, Babu D J & Venkateswarulu T C, 19 (2020) 100345.
69 Browne R B, Vishwakarma J N, Borah V V, Pegu R K & Roy J D, *In Data Science for Genomics*, (Elsevier, Academic Press) 2023, p. 107.
70 Cetin A, *Curr Comput Aided Drug Des*, 18 (2022) 337.
71 Zhao H & Caflisch A, *Eur J Med Chem*, 91 (2015) 4.
72 Pandey B, Grover A & Sharma P, *BMC Genomics*, 19 (2018) A132.
73 Schneider R, Sharma A R & Rai A A, *Introduction to molecular dynamics. In Computational Many-Particle Physics*, (Springer Berlin Heidelberg: Berlin, Heidelberg) 2008, p. 3.